Impact of a Model Soil Microorganism and of Its Secretome on the Fate of Silver Nanoparticles

Elise Eymard-Vernain, Cećile Lelong, Ana-Elena Pradas del Real, Romain Soulas, Sarah Bureau, Vanessa Tardillo Suarez, Benoit Gallet, Olivier Proux, Hiram Castillo-Michel, Géraldine Sarret

Impact of a model soil microorganism and of its secretome on the fate of silver nanoparticles

Eymard-Vernain Elise [1,2], Lelong Cécile [2], Pradas del Real Ana-Elena [1 3], Soulas Romain [4], Bureau Sarah [1], Tardillo Suarez Vanessa [5], Gallet Benoit [6], Proux Olivier [7 8] , Castillo-Michel Hiram [3] and Sarret Géraldine [1*]

1 ISTerre (Institut des Sciences de la Terre), Université Grenoble Alpes, CNRS, Grenoble, France

2 Université Grenoble Alpes, CEA Grenoble, Lab Chim & Biol Met, UMR CNRS CEA UJF, ProMD Team, BIG, Grenoble, France

3 ID21, ESRF-The European Synchrotron, CS40220, 38043 Grenoble, France

4 LITEN, CEA Grenoble, 17 Rue des Martyrs, 38054 Grenoble, France

5 ID16b, ESRF-The European Synchrotron, CS40220, 38043 Grenoble, France

6 Université Grenoble Alpes, CEA, CNRS, IBS, F-38000 Grenoble, France

7 Observatoire des Sciences de l'Univers de Grenoble (OSUG), UMR CNRS 832, Université Grenoble-Alpes, F-38041 Grenoble Cedex 9, France

8 BM30B/CRG-FAME, ESRF, Polygone scientifique Louis Néel, 71 avenue des Martyrs, 38000 Grenoble, France

Abstract

Sulfidation is a key process for silver nanoparticles released from consumer products in the environment. This study focuses on the impact of a model soil microorganism, *Bacillus subtilis*, on the fate of pristine and already sulfidized Ag-NPs. The nanoparticles were incubated with the initial growth medium, isolated secretome and living bacteria, and characterized for their size and morphology, agglomeration state, structure and Ag speciation. No Ag internalization or sorption on the cell wall was detected. A partial sulfidation, leading to an Ag-Ag_2S core-shell structure, was observed in the presence of the secretome, and the rate limiting step of the reaction was the oxidation of Ag^0, and it was favored near the crystal dislocations. The sulfidation was complete in the presence of the living bacteria and followed an indirect pathway. Both crystalline Ag_2S and amorphous Ag_2S and/or Ag-thiol were identified. At the opposite, the bacteria had no impact on Ag_2S. These results suggest that microorganisms participate to the sulfidation of Ag-NPs in aerobic systems such as unsaturated soils, and thus affect the bioavailability of Ag. It is important to take these transformations into account during exposure experiments, since they drastically change the exposure conditions. Finally, the secretome of *B. subtilis* might be used for the green synthesis of Ag-Ag_2S core-shell nanoparticles.

Introduction

Because of their broad-spectrum antimicrobial properties, silver nanoparticles (Ag-NPs) are increasingly produced and used in consumer products (cosmetics and personal care products, food and food packaging, textile, electronics) and also in medicine and agriculture.[1] This increased use has raised some concerns, both from a toxicological point of view for consumers during the use of these products, and from an ecotoxological point of view since Ag-NPs and their secondary products are expected to end up in environmental compartments, especially in soils, at the end of their life cycle.[2-3] Indeed, Ag-NPs released in wastewater accumulate in sewage sludge during wastewater treatment.[4] In Europe, 40 to 50% of this biosolid is applied on agricultural soils as amendment.[5]

Since the last decade, the ecotoxicity of Ag-NPs has been studied at various levels of complexity, from single organisms in growth media to complex systems such as soils and natural waters [6-7]. The impact on bacteria has been the focus of many studies since Ag-NPs are primarily used as biocides. This property results from several effect of Ag-NPs on bacteria including the generation of reactive oxygen species (ROS), the disruption of the membrane integrity, the interaction of Ag ions with proteins and disruption of their regular function, and the interference with DNA replication, causing DNA damage.[8-9] These effects are supposed to result mainly from the release of Ag ions by oxidative dissolution of the Ag-NPs. As a consequence, they are influenced by the physicochemical characteristics of the nanoparticles including the size, the shape and the nature of the coating.[10] The agglomeration state is another factor influencing the toxicity of Ag-NPs. The formation of agglomerates tends to decrease biocidal activity, possibly due to a decreased dissolution. Finally, chemical transformations likely modify the toxicity of Ag-NPs.[11] Sulfidation is a key process taking place in sewage

systems[12]and wastewater treatment plants.[4] This transformation decreases Ag-NPs toxicity, thanks to the low solubility of Ag_2S.[13-15] Sulfidation might also occur in growth media during *in vitro* exposure experiments, due to the composition of the growth medium itself, and to the release of thiol-containing molecules by the living organisms. To our knowledge, the impact of microorganisms' activity on the speciation of Ag-NPs in growth media has never been studied. Thus, it is important to assess the extent of these transformations, and to identify the agents responsible for these changes (the growth medium itself vs. the bacterial activity). Bacteria may also influence the chemical transformations of Ag-NPs in natural systems such as soils, especially in the rhizosphere. Studies on simplified systems can help to decipher the role of the various soil components in the NPs transformations.

The objective of this study was to characterize the physicochemical changes of Ag-NPs induced by a classical growth medium for bacteria (LB), by the molecules secreted by the bacteria, and by a living bacterial culture. The chosen strain is *Bacillus subtilis*, a model ~~soil~~ bacterium ubiquitous in the environment[16]. In soils, it plays a role in rhizospheric processes as a symbiotic organism for plants[17]. This Gram-positive bacterium secretes large amounts of proteins, peptides and amino acids.[18-19] It is actually used by the industry to produce biosurfactant, antifungal compounds, protease and poly-γ-glutamate.[19] Exposure conditions were chosen as close as possible to environmentally relevant conditions: Pristine and aged (i.e., sulfidized) Ag-NPs (referred to as Ag_2S-NPs), as well as Ag lactate as a control for ionic Ag were used, at a dose of 1 mg Ag L^{-1}. These various Ag forms were incubated in the initial growth medium, in the secretome without bacteria (supernatant after culture), and in the bacterial culture during the stationary phase. Although most exposure experiments are conducted during the exponential phase (e.g., [20-21]). The stationary phase, during which the medium is depleted in nutrients and when biopolymers and other exudates are present, is closer to the physiological state of bacteria in the environment.[22-23] A combination of analytical and

physical techniques were used, including dynamic light scattering (DLS), transmission electron microscopy coupled with energy dispersive X-ray spectrometry (TEM-EDX), nano X-ray fluorescence, bulk and nano X-ray absorption spectroscopy, and inductively coupled plasma – atomic emission spectrometry (ICP-AES).

Material and methods

Nanoparticles

The silver nanoparticles and silver lactate were purchased at Sigma: PVP-coated Ag-NPs (ref 758329, 5 wt% in ethylene glycol, <100 nm by TEM) and silver lactate (ref 85210, CH3CH(OH)COOAg, Molecular Weight: 196.94). Silver lactate was preferred to silver nitrate to avoid the formation of AgCl in the medium. Ag_2S-NPs were obtained by sulfidation of PVP-Ag-NPs as described in Levard et al.[24]. More details and characterization are provided in Figures S1 and S2.

Bacterial strain and culture media

The *B. subtilis* strain used was the 3610 strain (wild type) (personal gift, Maria Laaberki). The growth medium was LB: 10 $g.L^{-1}$ tryptone (Becton Dickinson ref: 212750), 5 g L^{-1} yeast extract (Becton Dickinson ref: 21705) and 5 g L^{-1} NaCl (Sigma: S9888). Isolation of the secretome: *Bacillus subtilis* strain 3610 was grown in Erlenmeyer flasks (250 mL) containing LB medium with an initial OD_{600} of 0.01 with shaking at 190 rpm at 37 °C. After 16h, the medium was depleted in nutrients from LB, and contained essentially the molecules secreted by the bacteria (> 10 g L-1 poly-γ–glutamate[25], 360 mg L^{-1} exopolysaccharides, 1 g L^{-1} DNA, and many proteins). Although the stationary phase was established since several hours, we did not observe significant cell mortality (as evaluated by lactate dehydrogenase assay). The

culture was centrifuged at 8000 rpm for 15 min, and the cell-free supernatant (SN), considered as the secretome, was recovered and used for incubations.

Incubations with Ag-NPs, Ag_2S-NPs and Ag lactate

Incubations with living bacteria: Cells were grown at 37°C in LB medium in 250 mL Erlenmeyer flasks during 16h with an initial OD_{600} of 0.01. After 16h of growth, the cells culture were further incubated alone (for the control) or with 1mg L^{-1} of Ag-NPs, or Ag_2S-NPs or 1.8 mg L^{-1} of silver lactate ((= 1mg L^{-1} of Ag) during 5h under shaking. Viability and central metabolism were not modified after exposure in these conditions (Eymard Vernain et al., subm). Incubations in LB and SN without bacterial cells: SN and LB media were incubated without (for the control) and with 1mg L^{-1} of Ag-NPs or Ag_2S-NPs or silver lactate during 5h at 37°C in 250 mL Erlenmeyer flasks filled up to 50 mL with shaking (referred to as "aerated condition", A, same as the bacterial culture), and in closed 50 mL falcon tubes (referred to as "unaerated condition", NA) at 25°C. These two conditions allowed us to test the influence of the aeration on the transformations.

Sample preparation after incubation

All samples were obtained after centrifugation at 8000 rpm for 30 min. Different sample preparations were used depending on the technique.

For TEM-EDX, samples without bacteria were deposited on a TEM copper grid (Ted Pella, ref 01824) and dried in inert atmosphere, and bacterial samples were fixed by high pressure freezing, freeze-substitution and resin embedding (Supporting Information), prepared as 400 nm sections and deposited on a TEM copper grid.

For nanoXRF/nanoXANES analyses, 400 nm sections of embedded bacteria were deposited on a grid with a Si3N4 window (Ted Pella, ref 21500-10). Other samples were prepared by

deposition of a drop of the fresh pellet on an ultralene film, drying in inert atmosphere, and fixation of this film on a PEEK sample holder.

For bulk EXAFS analysis, pellets were mixed with 20% glycerol as cryoprotectant, placed in the 5 mm diameter holes of the cryo-sample holder, plunged in liquid N_2, and introduced in frozen hydrated state in the cryostat. For Ag lactate samples, Ag could not be recovered by centrifugation, so the whole medium after incubation was freeze dried, diluted in BN and pressed into 5 mm diameter pellets.

TEM-EDX

Sample were observed using a Tecnai OSIRIS (FEI) in STEM mode operating at 200 kV with a probe current close to 0.7 nA. Elemental analysis was performed using four windowless energy dispersive X-ray detectors (Bruker) offering almost 1 srad of solid angle. Hyperspectral EDX maps were obtained, from which elemental profiles for S and Ag were extracted, and Ag/S peak intensity ratios were calculated. Diffraction patterns were recorded in TEM mode using selected area diffraction (SAD) technique.

NanoXRF

NanoXRF and XANES analyses were performed on beamline ID16b at the European Synchrotron Radiation Facility (ESRF, Grenoble, France). The optics used were a double white mirror with Pt coating and a KB mirrors system which focus the beam down to 62 (vertical) × 83 (horizontal) nm^2. Two fluorescence detectors (three-elements SDD arrays from SGX Sensortech) were used. The photon flux was 5.8×10^9 ph s^{-1} at 25.61 keV. NanoXRF maps were recorded at 25.61 keV, with a step size of 50 x 50 nm, and a dwell time of 100 ms.

X-ray absorption spectroscopy

Ag speciation was studied by Ag K-edge (25.5 keV) bulk EXAFS and XANES spectroscopy on FAME (BM30B) beamline at the ESRF and Samba beamline at SOLEIL synchrotron (Paris, France) at 15-20°K using a liquid He cryostat, by Ag L_{III}-edge (3.35 keV) bulk XANES spectroscopy on ID21 beamline at the ESRF at 80°K using a liquid N_2 cryostat, and by Ag K-edge nanoXANES spectroscopy at room temperature on ID16b beamline at the ESRF. Experimental details have been described previously for Ag K-edge bulk EXAFS on FAME[26] and Ag L_{III}-edge XANES on ID21[27]. For FAME and Samba data, a Si(220) monochromator, a 30- and 35-element, respectively, Ge detector were used. For Ag K-edge NanoXANES spectroscopy on ID16b, a Si(111) double crystal monochromator was used and spectra were recorded using the full XAS mapping mode.[28] S speciation was also studied by S K-edge XANES spectroscopy on ID21 (details in supporting information).

XANES and EXAFS data treatment was done with ATHENA from the Demeter software package.[29] After normalization, spectra were analyzed by linear combination fitting using libraries of Ag K- and L-edge and S K-edge references spectra detailed in Supporting Information.

ICP-AES

The intracellular silver was determined by ICP-AES after cell lysis (details in Supporting Information.

Dynamic light scattering (DLS)

Nanoparticles at 1 mg L^{-1} were incubated in ultrapure water (referred to as H_2O), LB medium or supernatant during 5 h in NA conditions before the DLS (dynamic light scattering)

measurement. The DLS apparatus was a DynaPro NanoStar (Wyatt Technology). Each measurement was performed at least on biological triplicates, and with four technical replicates. For each DLS analysis, between 2 and 5 hydrodynamic diameters were obtained. The results of the various measurements were plotted on the same figure, with no averaging. The absence of detectable particle in H_2O, LB and SN media was validated.

Statistical tests

Statistical tests (Tukey post hoc after ANOVA) were done on the EDX data (S/Ag peak heights) using the software SPSS.

Results

Distribution of silver in presence of *Bacillus subtilis*

Bacteria exposed to Ag-NPs, Ag_2S-NPs and Ag lactate were studied by nanoXRF in order to evaluate the possible internalization of Ag, or binding to the cell wall. Figure 1 shows the nanoXRF maps obtained on 400 nm sections of bacteria. Cells appear on the Os maps, thanks to OsO_4 staining (Os in Figure 1, details on freeze-substitution in Supporting information). For *B. subtilis* after exposure to Ag-NPs, Ag-rich spots of a few tens of nm, not in contact with bacteria, were observed. No concentrated or diffuse Ag was detected in the cytoplasm or cell wall of the bacteria. The detection limit for Ag in our experimental conditions is estimated to 27 ± 7 mg Ag L^{-1} (Supporting information). For *B. subtilis* after exposure to Ag_2S-NPs, aggregates of several micrometers of Ag_2S-NPs were observed in the medium. Beside this effect, there was no correlation between Ag and Os localization, suggesting no internalization of Ag. This finding was confirmed by analyzing bacteria far from the Ag_2S-NPs

aggregate, which shows the absence of silver (fourth row in Figure 1). Finally, for bacteria after exposure to Ag lactate, no Ag was detected inside and outside bacteria.

The absence of accumulation of silver in the bacteria for all conditions was confirmed by ICP-AES after cell lysis. Indeed, for all conditions, silver concentration in the samples after digestion was below the quantification limit of 3 µg L^{-1}, corresponding to 4.5 10^{-2} µg Ag per 15 mL tube. This amount corresponds to 0.018% of the initial Ag (1 mg L^{-1} in 250 mL of bacterial culture), to 4.5 attograms Ag per cell (considering about 10^{10} cells in 250 mL), and to an intracellular concentration of 8.6 mg L^{-1}. Bondarenko et al.[21] determined an intracellular concentration of 0.7 mg L^{-1} at the EC_{50} of *B. subtilis* exposed to Ag-NPs. The absence of toxicity observed in the present study suggests that the intracellular Ag concentration is below this value. A more sensitive method would be necessary to confirm this point. To sum up, for the three conditions, no internalization or association with the cell wall was observed, which is consistent with the absence of effects on the bacterial growth in our experimental conditions (Eymard Vernain et al., subm.).

After evaluating the possible internalization of Ag, we investigated the effects of *Bacillus subtilis* on the physicochemical state of the nanoparticles, and possible chemical transformations, by characterizing the Ag-NPs after incubation with the bacteria, and with the growth medium (LB) alone and the secretome (SN) alone.

Size and morphology of the NPs

The nominal size and morphological characteristics of Ag-NPs and Ag_2S-NPs were observed by transmission electron microscopy (TEM), after incubation for 5 h in H_2O, LB and SN (in NA conditions) and cell culture. Figure S3 shows representative images for these conditions, and compares the size distribution for Ag-NPs. A decrease in nominal size was observed between H_2O (majority of the nanoparticles between 40 and 80 nm) and LB or SN (majority of

NPs between 10 and 60 nm)(Figure S4). This observation suggests some partial dissolution of the Ag-NPs in LB and SN. In addition, TEM observation showed that the original and partly dissolved Ag-NPs were multi-twinned crystals (Figure S3 A-C). For the nanoparticles incubated with *B. subtilis*, there was no significant change in diameter compared to H_2O, but a dramatic change in morphology. Particles were actually aggregates of small (5 to 20 nm in diameter) single crystal nanoparticles (Figure S3).

Contrary to the Ag-NPs, Ag_2S-NPs produced by sulfidation with Na_2S formed aggregates between 350 nm and 10 µm, in which it was not possible to distinguish individual nanoparticles and to determine their nominal size (Figure S5).

Agglomeration state of Ag-NPs

The study of the agglomeration state by DLS was restricted to Ag-NPs since Ag_2S-NPs particles were not in a nano state (see below). Suspensions of Ag-NPs after incubation in H_2O, LB or SN in NA conditions were analyzed. For H_2O and LB, the DLS measurements were highly reproducible, and showed two populations: one with a diameter between 5 and 20 nm and the other one with diameter of about 100 nm (Figure S6). For SN, a variety of diameters, from a few nm to 1 µm, were obtained. Large diameters suggest an agglomeration due to SN, but the agglomeration state was not stable. Indeed, results were not reproducible. Figure S6 shows the various diameters obtained on the triplicate samples, with four analyses per sample. There results suggest that some molecules secreted by *Bacillus subtilis*, present in SN, induce an agglomeration of the silver nanoparticles.

The combination of DLS and TEM results suggest a partial dissolution of the individual nanoparticles in LB and SN, and their agglomeration in SN only.

TEM-EDX analyses

The Ag-NPs after incubation in the various media (H_2O, LB, SN, and bacterial culture) were then studied by TEM-EDX. This technique allowed imaging the distribution of S and Ag within the nanoparticles (Figure 2A). Different patterns were evidenced for Ag-NPs depending on the medium. With *Bacillus subtilis*, Ag and S distribution was uniform, with a Ag/S elemental ratio of 2/1, and SAED and HRTEM showed that the aggregates were composed of single crystals of acanthite (Ag_2S, Figure S7). Thus, Ag-NPs were sulfidized in the presence of bacteria. For Ag-NPs incubated in SN in aerated conditions, a coating of Ag_2S was observed, leading to an Ag-Ag_2S core-shell structure. The Ag_2S coating had a thickness of a few nm (Figure 2A and S8A), and was thicker near the dislocations of the multi-twinned Ag-NPs (Figure S9). HRTEM analyses showed that the Ag_2S shell was crystalline but surrounded by amorphous or organic phases (Figure S9). These observations suggest that the sulfidation occurs at the surface of the NPs, preferentially near the crystal defaults, possibly driven by some organic compounds. These observations suggest that the sulfidation progresses from the surface to the inner part of the NPs. This coating was less developed for SN in non-aerated conditions, even less for LB in aerated conditions (Figure 2A and Figure S8B), and almost absent for LB in non-aerated condition (Figure 2A). For Ag_2S-NPs after incubation of the various media (H_2O, SN, *B. subtilis*), a homogeneous distribution of Ag and S was observed, except in some localized regions with only Ag (Figure 2B). These areas are probably due to electron beam damage, since they increased in size with beam exposure. Moreover, bulk XRD analyzes of Ag_2S-NPs before incubation (Figure S1) and bulk XAS analyses after incubation (see next section) showed the absence of Ag^0 in these samples.

In order to compare more quantitatively the extent of sulfidation between the conditions, we extracted the EDX spectra of the whole NPs, and compared the height of the S peak after normalization to the height of the Ag peak for each condition (Figure 2C). As expected from the EDX maps, the S/Ag peak height increased in the order LB (NA) < SN (NA) < LB (A) <

SN (A) < *B. subtilis*. The difference was not significant for the first three, and significant ($p < 0.05$) for the latter two. The S/Ag peak was slightly lower for Ag-NPs + *B. subtilis* than for the Ag_2S-NPs reference. Thus, SN was more efficient at sulfidizing the NPs than LB, and aeration enhanced the sulfidation, but in all these conditions the sulfidation remained partial. Only the living bacteria led to an almost complete transformation to Ag_2S.

X-ray absorption spectroscopy

The nature and proportions of Ag species in each sample were then studied by X-ray absorption spectroscopy. XANES and EXAFS spectra, or XANES spectra only, were treated by LCFs using model compound spectra (Figure 3, Table 1). Principal component analysis was not used because the set of spectra at each edge was too small. Among the reference spectra of our K-edge database, four standards including Ag-NPs, Ag_2S-NPs, amorphous Ag_2S and Ag-thiol were sufficient to reproduce the spectra. Because of their similarity, the last two species were merged into a single pool. Although the LB medium contains 5 g L^{-1} NaCl, AgCl was not detected in any sample. No significant change in speciation was detected for Ag-NPs after incubation in LB or SN in NA conditions. By contrast, in A conditions, about 22% of sulfidation was detected for LB and 14 to 23% for SN (Table 1). The nature of the secondary species, either crystalline Ag_2S or amorphous Ag_2S/Ag-thiol, remains unclear for these samples because it is a minor phase (the error bar for this type of analysis is estimated at ± 10%). In the presence of *B. subtilis*, about 80% of Ag-NPs were sulfidized. The proportion of the secondary forms slightly differ between XANES and EXAFS LCFs (64 and 45% for crystalline Ag_2S, respectively, and 18 and 47% for amorphous Ag_2S/Ag and/or Ag-thiol, respectively, Table 1), but it remains clear that both species were present. The fit quality was clearly weaker (R factor increased by 20%) when only crystalline Ag_2S was used.

For silver lactate, the sulfidation was total in LB and SN, even in NA conditions. This is not surprising since Ag is already present as Ag^+, so there is no oxidation step required before

sulfidation. The final form was a mixture of crystalline Ag_2S and amorphous Ag_2S/Ag-thiol. A similar result was obtained for Ag lactate in the presence of *B. subtilis*. Again, fits were clearly weaker (R factor doubled) if only crystalline Ag_2S was used. Concerning Ag_2S-NPs, there was no significant change in speciation after incubation with *B. subtilis* and with SN in aerated conditions. The other conditions were not tested.

The speciation of sulfur in the LB medium before culture and in the supernatant after culture (in absence of silver) were studied by sulfur K-edge XANES spectroscopy **(**Figure S10). For both media, a mixture of thiols (R-SH), alkyl sulfides (R-S-R), sulfoxides (R-S=O) and sulfate were observed. The proportion of thiols was comparable in both media (26 to 32% of total S).

Discussion

Concerning the fate of pristine Ag-NPs in the various media, the molecules secreted by *B. subtilis* (SN medium) increased the agglomeration of Ag-NPs as compared to pure water, whereas the molecules of the initial growth medium (LB) did not. Meanwhile, a decrease of the particle nominal diameter, suggesting a partial dissolution, was observed after incubation with SN and LB. Although the toxicity of Ag-NPs strongly relies on their dissolution [21, 30-31], in our experimental conditions (1 mg L^{-1} Ag applied during the stationary phase), no impacts in terms of cell mortality or changes in the central metabolism of *Bacillus subtilis* were observed. This may be related to the presence of exopolymers produced by the bacteria known to decrease metals availability[32-33], and to other types of molecules excreted by the bacteria. This absence of toxicity is consistent with the absence of internalization of silver inside cells, as observed by nanoXRF and ICP-AES coupled with cell lysis. In addition, some transformations of Ag-NPs were observed, likely affecting Ag availability. Ag-NPs were partly sulfidized (about 20% of total Ag), and the secondary species (either crystalline Ag_2S or amorphous Ag_2S/Ag-thiol)

formed a homogeneous shell on the NPs, leading to an Ag-Ag_2S core-shell structure. Based on TEM-EDX results, this surface sulfidation was slightly higher in the medium containing the secretome (SN) than in the growth medium (LB). The aeration of the suspension, i.e., the presence of dissolved oxygen, clearly enhanced the reaction. The sulfidation of ionic silver (Ag lactate) in LB and SN was tested in non-aerated conditions. In that case the reaction was complete, with formation of crystalline Ag_2S and amorphous Ag_2S/Ag-thiol. These results allowed us to conclude that the limiting step of the sulfidation of Ag-NPs under our conditions was not the availability of reduced sulfur, but of oxygen, necessary for the oxidation of Ag^0 into Ag^+. After incubation with *Bacillus subtilis,* the sulfidation was almost complete (80%) and again, both crystalline Ag_2S (acanthite) and amorphous Ag_2S/Ag-thiol were formed, based on bulk XANES and EXAFS analysis. These results are in contradiction with those obtained by Hsueh et al. [34], who identified Ag_2O in a bacterial pellet of *B. subtilis* after exposure to 100 mg L-1 Ag-NPs. However, to our opinion these results are not valid since Ag_2S and Ag_2O reference spectra shown in this article are almost identical (which is not the case, e.g., [35]), and the first peak for the various references (Ag_2S, Ag_2O, Ag-NPs) are surprisingly at the same position.

The changes in speciation occurred without internalization or sorption on bacterial cell walls, as observed both from TEM-EDX and nanoXRF. The composite structure of the Ag_2S aggregates, composed of Ag_2S nanocrystals much smaller than the original Ag-NPs (Figure S3), suggest an indirect sulfidation, with release of Ag^+ ions followed by reaction with sulfides. On the contrary, a direct sulfidation was observed by Thalmann et al.[36] for Ag-NPs in the presence of HS^-, with the formation of hollow Ag_2S spheres attributed to the Kirkendall effect. Sulfidation of Ag-NPs can be realized by dissolved inorganic sulfide species including H_2S, HS^- and S^{2-}, and can be direct or indirect depending on the S/Ag ratio.[37] Inorganic sulfides are likely from the aerobic culture medium of a chemoheterotrophic strain like *B. subtilis*. Thus,

thiol-containing molecules present in the medium (as observed from S XANES spectroscopy) are the most likely sources of sulfide. This pathway would involve a cleavage of the S-C bond. Such cleavage has been documented in synthesis routes of nanosized Ag_2S using cysteine as S donor [38-39]. The proposed sulfidation mechanism is schematized in Figure S11.

These results show that living bacteria are more efficient at sulfidizing the Ag-NPs than the growth medium or secreted molecules alone. A possible explanation of this observation could be a modification of the secretome under Ag-NPs exposure. Indeed, the secretome used for the SN conditions is produced by the bacteria in the absence of Ag-NPs, and may differ from the one produced in the presence of Ag-NPs. Based on our conclusion on the rate limiting step of the sulfidation, we can hypothesize that the bacteria under Ag-NPs exposure excrete more oxidizing molecules. They might also excrete more thiol-containing molecules. These hypotheses could be tested by mass spectrometry proteomics experiments. Anyhow, an important result of this study is the demonstration that the bacterial activity has a strong impact on the fate of Ag-NPs.

Methodological and Environmental implications

This study shows that the bacterial activity has a major impact on the fate of Ag-NPs, by enhancing their sulfidation. The results suggest that the bacterial activity favors the first step of the reaction, which is the oxidation of Ag^0. Concerning the second step, the sulfidation itself, thiol-containing proteins and peptides are the most likely source of reduced S. These results suggest that microorganisms may participate to the sulfidation of Ag-NPs in aerobic systems in the environment, such as unsaturated soils. On the contrary, *B. subtilis* does not modify the speciation of Ag_2S-NPs.

This study has some implications for nano(eco)toxicology studies. In most studies, the NPs are characterized before the exposure experiment. Our study evidenced various extents of

chemical transformations of Ag-NPs after 5 hours of incubation, depending on the media. These changes clearly modify the exposure conditions. Thus, it is very important to monitor the speciation of NPs during exposure experiments. This type of information would clearly help the interpretation, and the inter comparison between studies. This point is valid for silver, and other NPs prone to transformations and/or redox reactions such as ZnO, CuO, CeO_2 for example.

In this study, Ag_2S-NPs produced by reacting Ag-NPs and Na_2S, was used as a proxy of aged Ag-NPs. These Ag_2S-NPs formed large aggregates (several tens of micrometers) of crystalline Ag_2S (acanthite), which were not altered in the presence of *Bacillus subtilis* or with their secreted molecules. This form clearly differed from the secondary products obtained after incubation of Ag-NPs with bacteria, which included both crystalline and amorphous Ag_2S and/or Ag-thiol, with particle size still in the nanometer range. In soils amended with sewage sludge, a mixture of crystalline and amorphous Ag_2S and/or Ag-thiol, present as micro and nanosized particles and as diffuse concentrations, was observed[26]. Thus, Ag_2S produced by reacting Ag-NPs and Na_2S may not be the most relevant material for toxicity studies since it is highly aggregated and fully crystalline. Sulfidation protocols involving thiol-containing molecules might provide more representative aged Ag-NPs.

The development of safer-by-design nanoparticles is a growing research topic. In the case of Ag-NPs, a decrease of the release of Ag from products (which can reach large amounts, for example for textiles[40-41]) while keeping the antibacterial properties, should be targeted. Partly sulfidized Ag-NPs, with an Ag-Ag_2S core-shell structure, such as those produced in this study, might be a material to test in this perspective. The secretome of *Bacillus subtilis* may have some potential for the green synthesis of these nanocomposites.

Supporting Information

Materials and Methods: Nanoparticles characterization, high pressure freezing and freeze-substitution, Ag reference compounds for XAS analyses, nanoXRF detection limit, ICP-AES after cell lysis. Results: DLS analyses, TEM coupled with EDX, electron diffraction and high resolution, S K-edge XANES and proposed mechanism of sulfidation of Ag-NPs in the presence of *B. subtilis* (Figures S3 to S11). All data are presented in a single PDF document.

Acknowledgments

The authors thank the French program LabEx Serenade (11-LABX-0064) for providing a PhD fellowship and EquipEx NanoID (ANR-10-EQPX-39) for funding the TEM Osiris used in this study. ISTerre is also part of Labex OSUG@2020 (ANR10 LABX56). The authors thank ESRF and Soleil synchrotrons for providing beam time. The beamline staff of FAME, ID16b and ID21 (ESRF) and Samba (Soleil) are acknowledged for their help in collecting data. Giulia Veronesi is acknowledged for the S XANES measurements on ID21, and Alexandre Gelabert, Morgane Desmau and Clément Levard are acknowledged for recording the data on Samba beamline. We thank Christine Moriscot for her help on TEM sample preparation, realized on the platforms of the Grenoble Instruct-ERIC Center (ISBG : UMS 3518 CNRS-CEA-UGA-EMBL) with support from FRISBI (ANR-10-INSB-05-02) and GRAL (ANR-10-LABX-49-01) within the Grenoble Partnership for Structural Biology (PSB). The electron microscope facility used for TEM sample preparation is supported by the Rhône-Alpes Region, the Fondation Recherche Medicale (FRM), the fonds FEDER and the GIS-Infrastrutures en Biologie Sante et Agronomie (IBISA).

References

(1) Pulit-Prociak, J.; Stoklosa, K.; Banach, M., Nanosilver products and toxicity. *Environmental Chemistry Letters* **2015,** *13* (1), 59-68.

(2) Gottschalk, F.; Sonderer, T.; Scholz, R. W.; Nowack, B., Modeled environmental concentrations of engineered nanomaterials (TiO2, ZnO, Ag, CNT, fullerenes) for different regions. *Environ. Sci. Technol.* **2009,** *43*, 9216-9222.

(3) Sun, T. Y.; Gottschalk, F.; Hungerbuehler, K.; Nowack, B., Comprehensive probabilistic modelling of environmental emissions of engineered nanomaterials. *Environ. Pollut.* **2014,** *185*, 69-76.

(4) Kaegi, R.; Voegelin, A.; Sinnet, B.; Zuleeg, S.; Hagendorfer, H.; Burkhardt, M.; Siegrist, H., Behavior of metallic silver nanoparticles in a pilot wastewater treatment plant. *Environ. Sci. & Technol.* **2011,** *45* (9), 3902-3908.

(5) Kelessidis, A.; Stasinakis, A. S., Comparative study of the methods used for treatment and final disposal of sewage sludge in European countries. *Waste Management* **2012,** *32* (6), 1186-1195.

(6) Navarro, E.; Baun, A.; Behra, R.; Hartmann, N. B.; Filser, J.; Miao, A. J.; Quigg, A.; Santschi, P. H.; Sigg, L., Environmental behavior and ecotoxicity of engineered nanoparticles to algae, plants, and fungi. *Ecotoxicology* **2008,** *17* (5), 372-386.

(7) Maillard, J.-Y.; Hartemann, P., Silver as an antimicrobial: facts and gaps in knowledge. *Crit. Rev.Microbiol.* **2013,** *39* (4), 373-383.

(8) Niazi, J. H.; Gu, M. B., Toxicity of Metallic Nanoparticles in Microorganisms- a Review. In *Atmospheric and Biological Environmental Monitoring*, Kim, Y. J.; Platt, U.; Gu, M. B.; Iwahashi, H., Eds. Springer Netherlands: Dordrecht, 2009; pp 193-206.

(9) Duran, N.; Duran, M.; de Jesus, M. B.; Seabra, A. B.; Favaro, W. J.; Nakazato, G., Silver nanoparticles: A new view on mechanistic aspects on antimicrobial activity. *Nanomedicine-Nanotechnology Biology and Medicine* **2016,** *12* (3), 789-799.

(10) Marambio-Jones, C.; Hoek, E. M. V., A review of the antibacterial effects of silver nanomaterials and potential implications for human health and the environment. *J. Nanopart. Res.* **2010,** *12* (5), 1531-1551.

(11) Reidy, B.; Haase, A.; Luch, A.; Dawson, K.; Lynch, I., Mechanisms of Silver Nanoparticle Release, Transformation and Toxicity: A Critical Review of Current Knowledge and Recommendations for Future Studies and Applications. *Materials* **2013,** *6* (6), 2295.

(12) Kaegi, R.; Voegelin, A.; Ort, C.; Sinnet, B.; Thalmann, B.; Krismer, J.; Hagendorfer, H.; Elumelu, M.; Mueller, E., Fate and transformation of silver nanoparticles in urban wastewater systems. *Water Research* **2013,** *47* (12), 3866-3877.

(13) Levard, C.; Hotze, E. M.; Lowry, G. V.; Brown, G. E., Environmental Transformations of Silver Nanoparticles: Impact on Stability and Toxicity. *Environ. Sci. Technol.* **2012,** *46* (13), 6900-6914.

(14) Levard, C.; Hotze, E. M.; Colman, B. P.; Dale, A. L.; Truong, L.; Yang, X. Y.; Bone, A. J.; Brown, G. E.; Tanguay, R. L.; Di Giulio, R. T.; Bernhardt, E. S.; Meyer, J. N.; Wiesner, M. R.; Lowry, G. V., Sulfidation of silver nanoparticles: Natural antidote to their toxicity ? *Environ. Sci. Technol.* **2013,** *47* (23), 13440-13448.

(15) Yu, S. J.; Yin, Y. G.; Liu, J. F., Silver nanoparticles in the environment. *Environmental Science-Processes & Impacts* **2013,** *15* (1), 78-92.

(16) Earl, A. M.; Losick, R.; Kolter, R., Ecology and genomics of Bacillus subtilis. *Trends in Microbiology 16* (6), 269-275.

(17) Pandey, A.; Palni, L. M. S., Bacillus species: The dominant bacteria of the rhizosphere of established tea bushes. *Microbiological Research* **1997,** *152* (4), 359-365.

(18) Marvasi, M.; Visscher, P. T.; Casillas Martinez, L., Exopolymeric substances (EPS) from Bacillus subtilis : polymers and genes encoding their synthesis. *FEMS Microbiology Letters* **2010,** *313* (1), 1-9.

(19) van Dijl, J.; Hecker, M., Bacillus subtilis: from soil bacterium to super-secreting cell factory. *Microbial Cell Factories* **2013,** *12* (1), 3.

(20) Kim, S. W.; Baek, Y.-W.; An, Y.-J., Assay-dependent effect of silver nanoparticles to Escherichia coli and Bacillus subtilis. *Applied Microbiology and Biotechnology* **2011,** *92* (5), 1045-1052.

(21) Bondarenko, O.; Ivask, A.; Kakinen, A.; Kurvet, I.; Kahru, A., Particle-Cell Contact Enhances Antibacterial Activity of Silver Nanoparticles. *Plos One* **2013,** *8* (5).

(22) Völker, U.; Hecker, M., From genomics via proteomics to cellular physiology of the Gram-positive model organism Bacillus subtilis. *Cellular Microbiology* **2005,** *7* (8), 1077-1085.

(23) Overkamp, W.; Ercan, O.; Herber, M.; van Maris, A. J. A.; Kleerebezem, M.; Kuipers, O. P., Physiological and cell morphology adaptation of Bacillus subtilis at near-zero specific growth rates: a transcriptome analysis. *Environmental Microbiology* **2015,** *17* (2), 346-363.

(24) Levard, C.; Reinsch, B. C.; Michel, F. M.; Oumahi, C.; Lowry, G. V.; Brown, G. E., Sulfidation Processes of PVP-Coated Silver Nanoparticles in Aqueous Solution: Impact on Dissolution Rate. *Environ. Sci. Technol.* **2011,** *45* (12), 5260-5266.

(25) Zeng, W.; Chen, G.; Wu, H.; Wang, J.; Liu, Y.; Guo, Y.; Liang, Z., Improvement of Bacillus subtilis for poly-γ-glutamic acid production by genome shuffling. *Microbial Biotechnology* **2016,** *9* (6), 824-833.

(26) Pradas del Real, A. E.; Castillo-Michel, H.; Kaegi, R.; Sinnet, B.; Magnin, V.; Findling, N.; Villanova, J.; Carriere, M.; Santaella, C.; Fernandez-Martinez, A.; Levard, C.; Sarret, G., Fate of Ag-NPs in sewage sludge after application on agricultural soils. *Environ. Sci. Technol.* **2016,** *50* (4), 1759-1768.

494 (27) Pradas del Real, A. E.; Vidal, V.; Carrière, M.; Castillo-Michel, H.; Levard, C.; Chaurand, P.;
495 Sarret, G., Silver Nanoparticles and Wheat Roots: A Complex Interplay. *Environ. Sci. Technol.* **2017,** *51*
496 (10), 5774-5782.
497 (28) Castillo-Michel, H.; Larue, C.; Pradas del Real, A.-E.; Cotte, M.; Sarret, G., Practical review on
498 the use of synchrotron based micro- and nano- X-ray fluorescence mapping and X-ray absorption
499 spectroscopy to investigate the interactions between plants and engineered nanomaterials. *Plant*
500 *Physiol. Biochem.* **2017,** *110*, 13-32.
501 (29) Ravel, B.; Newville, M., ATHENA and ARTEMIS: Interactive graphical data analysis using IFEFFIT.
502 *J. Synchr. Rad.* **2005,** *12*, 537-541.
503 (30) Ivask, A.; Kurvet, I.; Kasemets, K.; Blinova, I.; Aruoja, V.; Suppi, S.; Vija, H.; Käkinen, A.; Titma,
504 T.; Heinlaan, M.; Visnapuu, M.; Koller, D.; Kisand, V.; Kahru, A., Size-Dependent Toxicity of Silver
505 Nanoparticles to Bacteria, Yeast, Algae, Crustaceans and Mammalian Cells In Vitro. *PLOS ONE* **2014,** *9*
506 (7), e102108.
507 (31) Agnihotri, S.; Mukherji, S.; Mukherji, S., Size-controlled silver nanoparticles synthesized over
508 the range 5-100 nm using the same protocol and their antibacterial efficacy. *RSC Advances* **2014,** *4* (8),
509 3974-3983.
510 (32) Li, C. C.; Wang, Y. J.; Dang, F.; Zhou, D. M., Mechanistic understanding of reduced AgNP
511 phytotoxicity induced by extracellular polymeric substances. *J. Hazardous Mat.* **2016,** *308*, 21-28.
512 (33) Koser, J.; Engelke, M.; Hoppe, M.; Nogowski, A.; Filser, J.; Thoming, J., Predictability of silver
513 nanoparticle speciation and toxicity in ecotoxicological media. *Environmental Science-Nano* **2017,** *4*
514 (7), 1470-1483.
515 (34) Hsueh, Y.-H.; Lin, K.-S.; Ke, W.-J.; Hsieh, C.-T.; Chiang, C.-L.; Tzou, D.-Y.; Liu, S.-T., The
516 Antimicrobial Properties of Silver Nanoparticles in <italic>Bacillus subtilis</italic> Are Mediated by
517 Released Ag⁺ Ions. *PLOS ONE* **2015,** *10* (12), e0144306.
518 (35) Yin, L.; Cheng, Y.; Espinasse, B.; Colman, B. P.; Auffan, M.; Wiesner, M.; Rose, J.; Liu, J.;
519 Bernhardt, E., More than ions: the effects of silver nanoparticles on Lolium multiflorum. *Environ. Sci.*
520 *Technol.* **2011,** *45*, 2360-2367.
521 (36) Thalmann, B.; Voegelin, A.; Morgenroth, E.; Kaegi, R., Effect of humic acid on the kinetics of
522 silver nanoparticle sulfidation. *Environmental Science-Nano* **2016,** *3* (1), 203-212.
523 (37) Liu, J. Y.; Pennell, K. G.; Hurt, R. H., Kinetics and Mechanisms of Nanosilver Oxysulfidation.
524 *Environ. Sci. Technol.* **2011,** *45* (17), 7345-7353.
525 (38) Xiang, J.; Cao, H.; Wu, Q.; Zhang, S.; Zhang, X.; Watt, A. A. R., l-Cysteine-Assisted Synthesis and
526 Optical Properties of Ag2S Nanospheres. *The Journal of Physical Chemistry C* **2008,** *112* (10), 3580-
527 3584.

(39) Banerjee, S.; Show, B.; Kundu, A.; Ganguly, J.; Gangopadhyay, U.; Saha, H.; Mukherjee, N., N-acetyle cysteine assisted synthesis of core-shell Ag2S with enhanced light transmission and diminished reflectance: Surface modifier for c-SiNx solar cells. *Journal of Industrial and Engineering Chemistry* **2016,** *40*, 54-61.

(40) Lorenz, C.; Windler, L.; von Goetz, N.; Lehmann, R. P.; Schuppler, M.; Hungerbuhler, K.; Heuberger, M.; Nowack, B., Characterization of silver release from commercially available functional (nano)textiles. *Chemosphere* **2012,** *89* (7), 817-824.

(41) Mitrano, D. M.; Rimmele, E.; Wichser, A.; Erni, R.; Height, M.; Nowack, B., Presence of Nanoparticles in Wash Water from Conventional Silver and Nano-silver Textiles. *ACS Nano* **2014,** *8* (7), 7208-7219.

539

Table 1 : Distribution of Ag species determined by linear combination fitting of XAS spectra

Samples	Molar percentage of Ag species			Sum	R factor[a]	Edge, type of data and temp. of acquisition
	Ag-NPs	Ag_2S-NPs	Amorphous Ag_2S or Ag-thiol			
Ag-NPs incubated with:						
B. subtilis	17	64	18	99	0.0003	K, XANES, 15°K
	19	45	47	111	0.1554	K, EXAFS, 15°K
LB **(NA)** [b]	100			100	0.0005	K, XANES, 15°K
	100			100	0.0310	K, EXAFS, 15°K
LB **(A)** [c]	78	22	n.t. [d]	100	0.0017	K, XANES, RT
SN **(NA)**	100			100	0.0003	K, XANES, 15°K
	100			100	0.0836	K, EXAFS, 15°K
SN-1 **(A)**	77	23	n.t.	100	0.0017	K, XANES, RT
SN-2 **(A)**	100			100	0.0400	K, XANES, 15°K
	90		15	105	0.0400	K, EXAFS, 15°K
SN-3 **(A)**	89		14	103	0.0080	L, XANES, 80°K
Ag_2S-NPs incubated with:						
B. subtilis		100		100	0.0005	L, XANES, 80°K
SN **(A)**	7	91	n.t.	98	0.0002	K, XANES, RT
SN-2 **(A)**		100		100	0.0003	L, XANES, 80°K
Ag lactate incubated with:						
B. subtilis		25	72	97	0.0030	K, XANES, 15°K
LB **(NA)**		42	58	100	0.0008	K, XANES, 15°K
SN **(NA)**		32	68	100	0.0008	K, XANES, 15°K

Fits were done in the [E_0-20; E_0+80] eV range for XANES spectra, and in the [2-12] $Å^{-1}$ range for EXAFS spectra. Up to three components were used, except for XANES spectra recorded at RT, for which only two-components (Ag-NPs and Ag2S-NPs) were used. [a] Fit quality criterion provided by ATHENA (R factor = $\Sigma [k^2 \chi_{exp} - k^2 \chi_{fit}]^2 / \Sigma [k^2 \chi_{exp}]^2$ for EXAFS spectra, and $\Sigma [\mu_{exp} - \mu_{fit}]^2 / \Sigma [\mu_{exp}]^2$ for XANES spectra. [b] Non-aerated conditions, [c] Aerated conditions. [d] Not tested because of the absence of these reference spectra in the K-edge database at RT. LB: initial growth medium. SN: supernatant (three replicates analyzed for Ag-NPs, aerated conditions).

540

541

Figure captions

Figure 1: Nano-XRF analysis of *Bacillus subtilis* after incubation with Ag-NPs, Ag_2S-NPs, and Ag lactate. The bacteria are imaged using the Os signal. Max number of counts for Os and Ag are given for each map. Scale bar: 1µm. step size: 0.05*0.05 µm, dwell time: 500ms

Figure 2: Ag (red), S (green) and Ag + S elemental maps obtained by TEM-EDX for the Ag-NPs after incubation in H_2O, LB, SN, and with bacteria in aerated (A) or non-aerated (NA) condition (Fig. 2A) and for Ag_2S-NPs after 5h incubation in H_2O, SN and with bacteria (Fig. 2B). Scale bar: 50 nm. (C) Comparison of the S/Ag peak height of the EDX spectra for individual NPs, extracted from the maps. Significant differences according to the Tukey test ($p< 0.05$) are indicated by letters.

Figure 3: XAS spectra for Ag reference compounds and samples, recorded in various conditions: A, B: Bulk Ag K-edge XANES (A) spectra and EXAFS (B) spectra recorded at 15°K. C: nano Ag K-edge XANES spectra recorded at room temperature. D: bulk Ag L_{III}-edge XANES spectra recorded at 80°K. For the samples, the color of the spectra correspond to the initial Ag form: Ag-NPs in red, Ag_2S-NPs is green, and Ag lactate in grey. Linear combination fitting are shown in blue dashed lines.

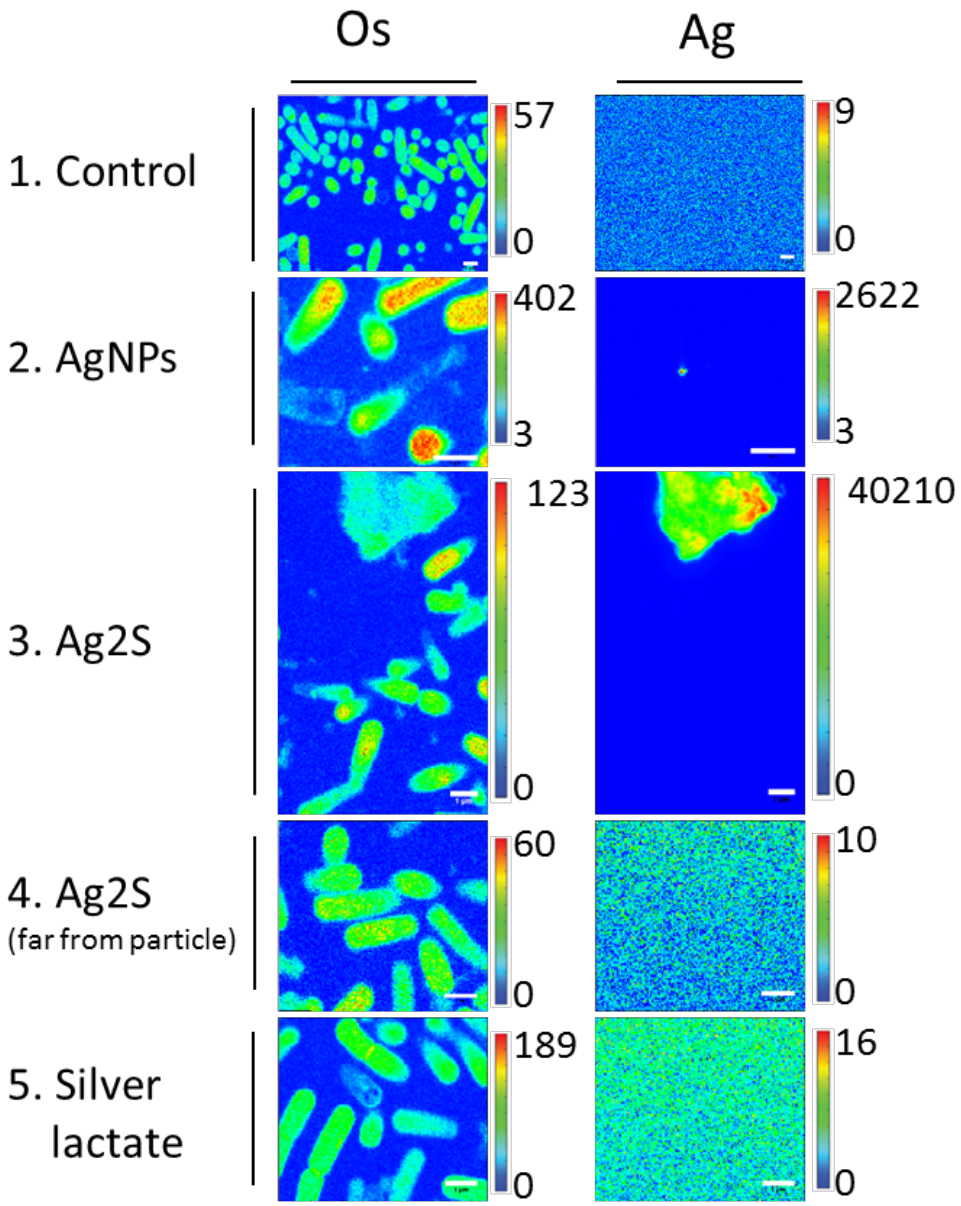

562

563 **Figure 1**

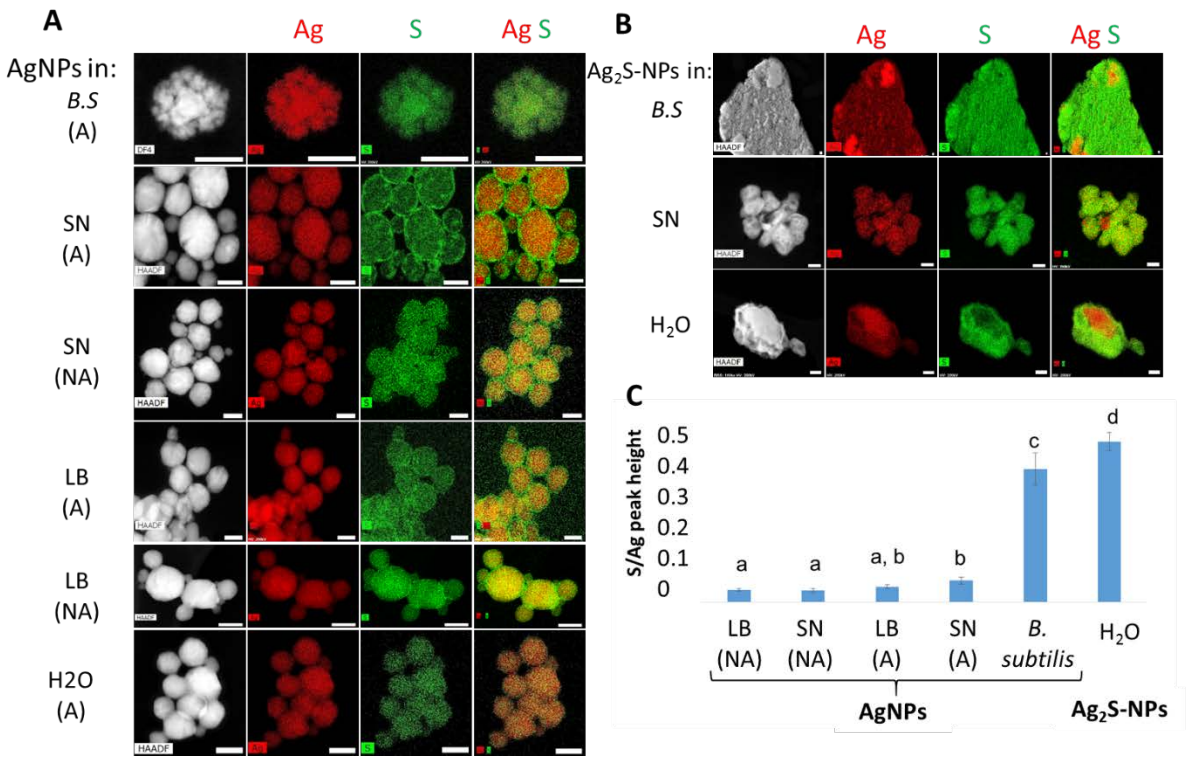

564

565 **Figure 2**

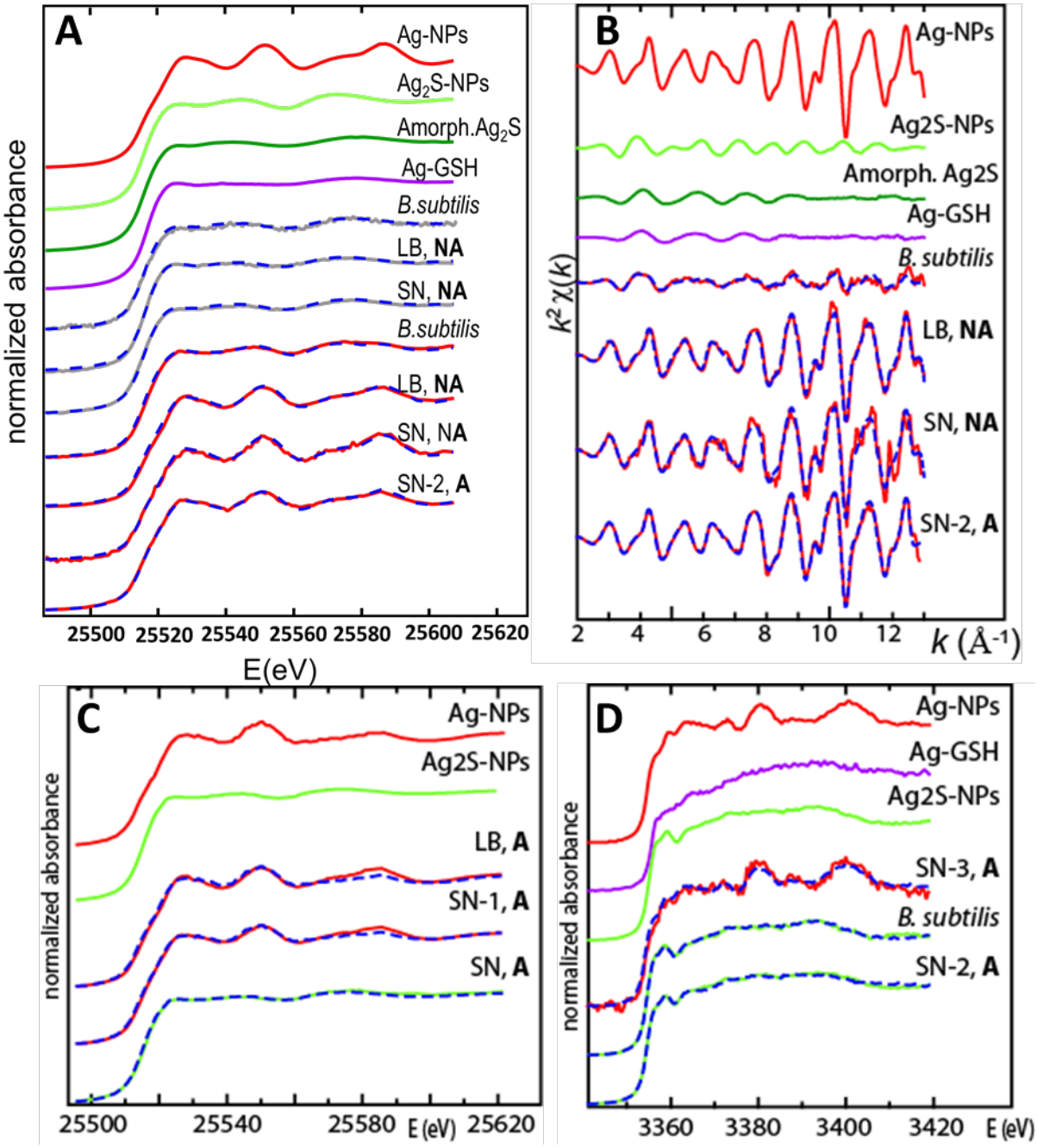
A
Ag-NPs
Ag2S-NPs
Amorph.Ag2S
Ag-GSH
B.subtilis
LB, NA
SN, NA
B.subtilis
LB, NA
SN, NA
SN-2, A
normalized absorbance
25500 25520 25540 25560 25580 25600 25620
E(eV)
B
Ag-NPs
Ag2S-NPs
Amorph. Ag2S
Ag-GSH
B. subtilis
LB, NA
SN, NA
SN-2, A
k² χ(k)
2 4 6 8 10 12
k (Å⁻¹)
C
Ag-NPs
Ag2S-NPs
LB, A
SN-1, A
SN, A
normalized absorbance
25500 25540 25580 E (eV) 25620
D
Ag-NPs
Ag-GSH
Ag2S-NPs
SN-3, A
B. subtilis
SN-2, A
normalized absorbance
3360 3380 3400 3420 E (eV)

Figure 3